Supplement for Satellite Observations Reveal Northern California Wildfire Aerosols Reduce Cloud Cover in California and Nevada Through Semi-Direct Effects

James L. Gomez[1], Robert J. Allen[1], and King-Fai Li[1]

[1]University of California, Riverside

Correspondence: James Gomez (jgome222@ucr.edu)

1 Additional Method Verification with Correlations

The methods for this paper were employed as typical cross correlations would not be able to differentiate effects of fires from fire weather, and on a daily scale cross correlations are not possible due to missing data. However, the results of the double stratification should be reflected in monthly cross correlation between nCA DM and the variables of interest. Verification of the methods of this paper are needed, because though they are consistent with previous hypotheses that the semi-direct effect can influence radiative forcing over the western US (Liu et al., 2014), they go against the hypothesis that fires fires may create clouds through increasing specific humidity through invigorated convection at the site of the fire and release of fuel moisture (Kim & Sarkar, 2017; Liu et al., 2014). Correlations between DM and AOD, as well as between DM and cloud layer water mass mixing ratio $M_{H_2O(cl)}$ over the site of DM emission (gridcell-by-gridcell) indicate that fires are much more strongly associated with increases in AOD than $M_{H_2O(cl)}$ (**Figure S4a,b**). When repeating this process with nCA DM x AOD/$M_{H_2O(cl)}$, it becomes evidently clear that fires in nCA may have a small negative impact on $M_{H_2O(cl)}$, but are associated with widespread increases in AOD **Figure S4c,d**. As depicted in **Figure 1b** and **Figure 4b,c**, no matter how the data is stratified, the increase in AOD witnessed in the method utilized in this paper is consistent with monthly cross correlations. Finally, **Figure 9** was replicated with the monthly cross correlation method. This yielded results consistent with the methods utilized in this paper (**Figure S5**). **Figure S5** showcases that the warming of the cloud layer and corresponding reduction in RH and CF are comparable spatially to that of **Figure 9**. However, though **Figure S4d** shows generally negative correlations between nCA DM and $M_{H_2O(cl)}$, these correlations are not significant in nCA-NV. Therefore, there is higher confidence in the results that the fires decrease cloud cover through direct reduction of RH through warming rather than through altering specific humidity. Consistency between the stratification method as well as the monthly cross correlation method indicate that the temporal error introduced by using GFED DM is in fact negligible, and that the method utilized in this paper is sound. Additionally, this analysis indicates that any small scale instantaneous increases in specific humidity are quickly overpowered by the semi-direct effects described in this paper. Further analysis on specific humidity change over fire site can be found in the supplement.

2 Changes in Circulation

2.1 MERRA-2

The Modern-Era Retrospective analysis for Research and Applications, Version 2 (MERRA-2) 3-hourly reanalysis dataset (Global Modeling And Assimilation Office & Pawson, 2015) was used to analyze profiles of vertical pressure velocity Ω as well as both longitudinal and latitudinal wind speed. MERRA-2 assimilates data from a plethora of satellites into the Goddard Earth Observing System, version 1 (GEOS-1) model to obtain a historical record of climate data (Gelaro et al., 2017). As the data is of a resolution of 361x576x46x8 (latitude by longitude by vertical pressure level by time), it had to be processed into a daily 1 degree grid. This was accomplished by averaging the 3-hourly data into daily data, and then performing linear interpolation to the MODIS 1 degree grid.

2.2 Changes in Pressure velocity Ω

The decreases in high troposphere M_{H_2O} are coincident with significant decreases in Ω, which corresponds to weakened downdrafts or strengthened updrafts. **Figure S8a,b** depict high minus low DM Ω anomaly profiles over the nCA-NV region during high and low p_s extremes respectively. Each profile depicts consistently negative Ω anomalies, but for high p_s these changes are only significant in the low troposphere while for high p_s the changes are only significant in the high troposphere. **Figure S8c,d** depict high minus low DM high troposphere Ω anomalies for high and low p_s extremes respectively. **Figure S8c,d** demonstrate that the negative high troposphere Ω anomalies are larger in magnitude under low p_s extremes compared to high p_s extremes. Additionally, the spatial distribution of the largest negative Ω anomalies are consistent with the decreases in M_{H_2O} in **Figure 6a**. This implies that part of the decrease in RH in the high troposphere may be due to a change in the vertical transport of moisture.

2.3 Changes in Wind Vectors

In **Figure 6a**, it is noted that there is a significant decrease in M_{H_2O} in the high troposphere over northern Nevada. Additionally, there is a significant increase in M_{H_2O} in southern Nevada as well as in southwestern Utah. Also of note, there is an increase in CF_{lw} in southwestern Utah. Therefore, it appears possible that there is a transport of moisture from the high troposphere to the lower troposphere in southern Nevada/southwestern Utah. **Figure S9** depicts low pressure extreme high fire minus low fire days' MERRA-2 wind vector and wind speed anomalies in the high troposphere. Overall, there appears to be a strong northeasterly wind anomaly from the high troposphere over northern Nevada that points towards southern Nevada/southwestern Utah. This implies that part of the decrease in RH and CF_{cir} over northern Nevada is potentially due to wind patterns that transport moisture out of the high troposphere to the lower troposphere elsewhere. It is unknown if this change in wind speed is due to warming from the aerosols, or if these wind patterns are an artifact that was not filtered out from analyzing low p_s conditions. However, the changes in latitudinal wind speeds correlate significantly with AOD spatially **Figure S9b**.

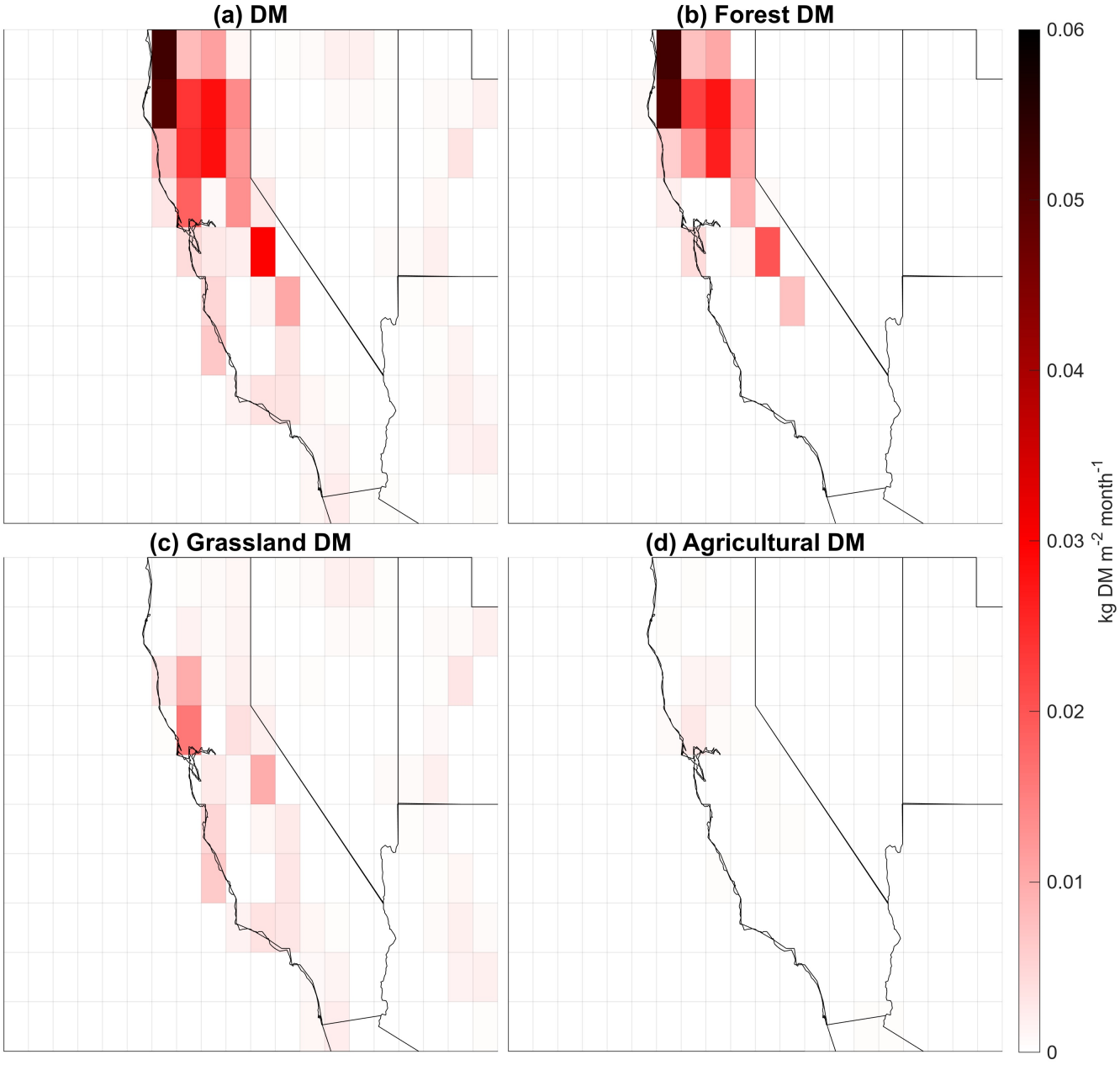

Figure S1. 20-year seasonal average fire dry matter (DM) emissions per biome over the south western US. 2003-2022 June-October seasonal average DM emissions for (a) all biomes, (b) temperate forests, (c) grasslands, and (d) agricultural land. The majority of dry matter emissions come from temperate forests, followed by grasslands, then agricultural lands contribute minimally to net DM emissions.

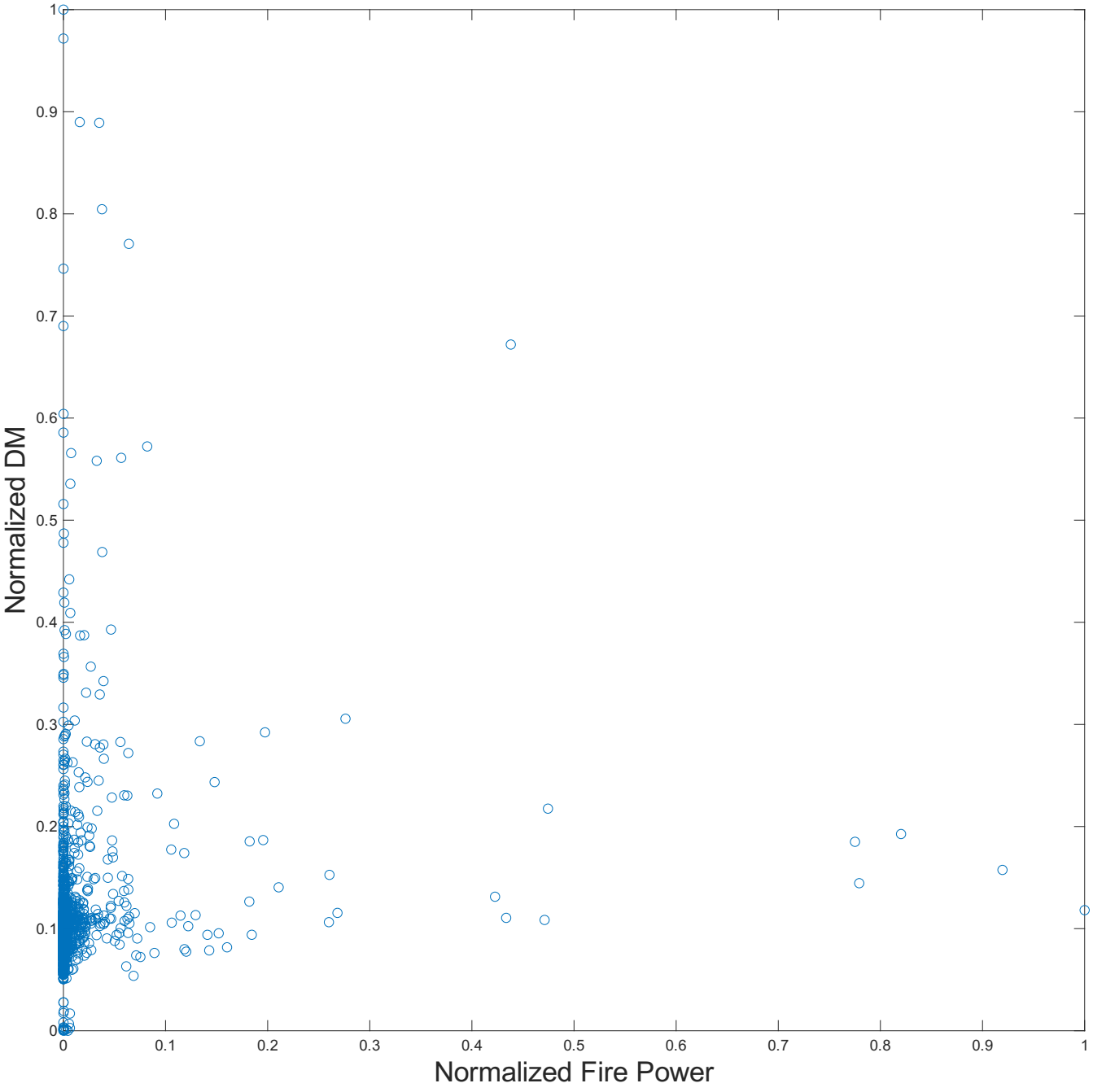

Figure S2. Normalized daily Global Fire Emission Database v4 dry matter emissions DM vs normalized daily MODIS Aqua fire power (FP) in northern California. Data consists of all available days within 2003-2022 fire seasons for both datasets. If using each variable as a metric of fire emission, MODIS Aqua FP systematically underestimates days of high fire emission relative to GFED DM. This is likely due to cloud cover obstructing daily FP retrievals in MODIS, and due to vegetation type being important for fire emission estimation.

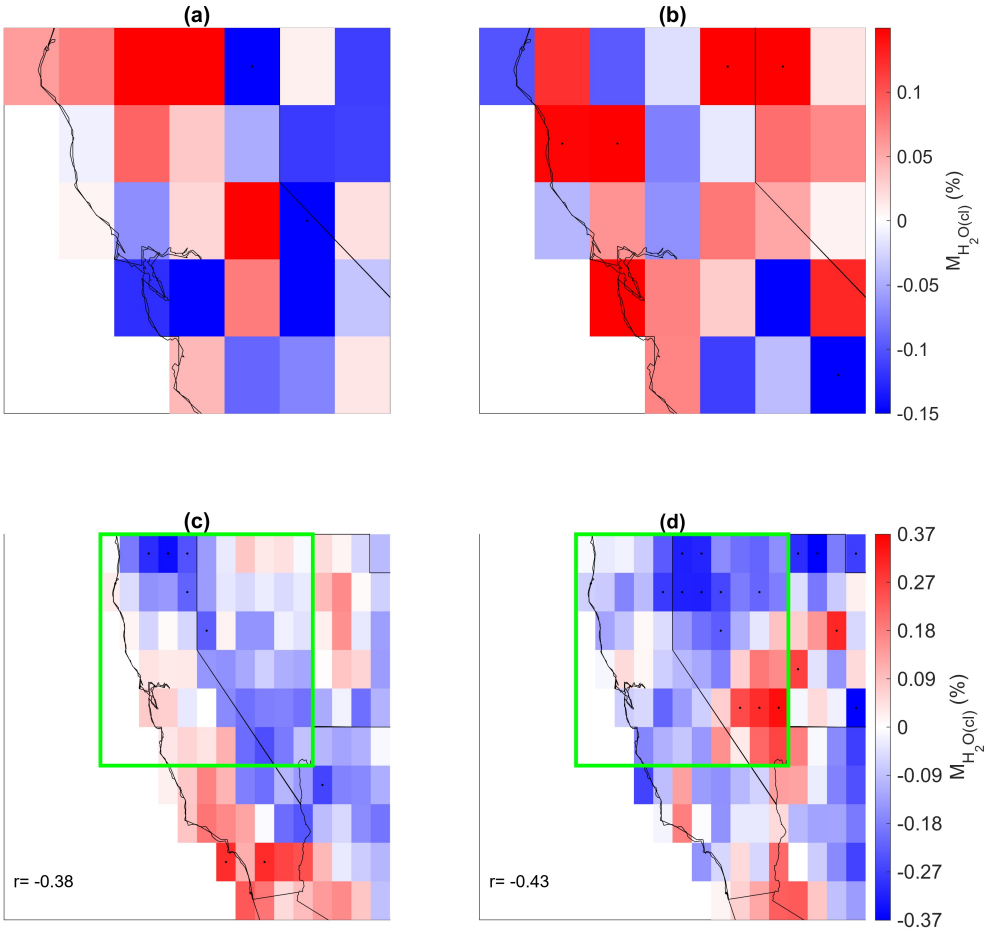

Figure S3. Small scale and large scale differences in cloud layer (700hPa-250hPa) water mass mixing ratio ($M_{H_2O(cl)}$) between high and low fire dry matter emission DM conditions. (a) and (b) depict $M_{H_2O(cl)}$ anomalies stratified by 90th minus 10th percentile DM on a gridcell by gridcell basis for high (a) and low (b) surface pressure p_s conditions in northern California (nCA) in the 2003-2022 June-October time frame. (a) and (b) capture the effects that fires have on their gridcell's $M_{H_2O(cl)}$. (c) and (d) depict $M_{H_2O(cl)}$ stratified by regional average nCA 90th percentile minus 10th percentile regional average nCA DM days in each gridcell for high (c) and low (d) p_s conditions in the 2003-2022 June-October time frame. (c) and (d) showcase the effects of fires in nCA on the rest of the region's $M_{H_2O(cl)}$. (a) shows that during high p_s and high DM conditions, on a small scale there is a preference for negative cloud layer $M_{H_2O(cl)}$ over the fire's gridcell, with two significantly negative gridcells, and a majority of gridcells in the region being negative. (b) indicates that during high p_s and high DM conditions, on a small scale there is a preference for positive cloud layer $M_{H_2O(cl)}$ over the fire's gridcell, with four significantly positive gridcells, and a majority of gridcells in the region being positive. Two of the significantly positive cells in (b) are also two of the highest DM gridcells in the region (**Figure 1a**). Figures (c) and (d) indicate that when fires are occurring in nCA, there is no resulting increase in $M_{H_2O(cl)}$ in the northern California-Nevada region (green box). In fact, there are decreases. Therefore, while low p_s conditions overall correspond with an increase in specific humidity at the fire site, this does not translate to increases elsewhere in the region.

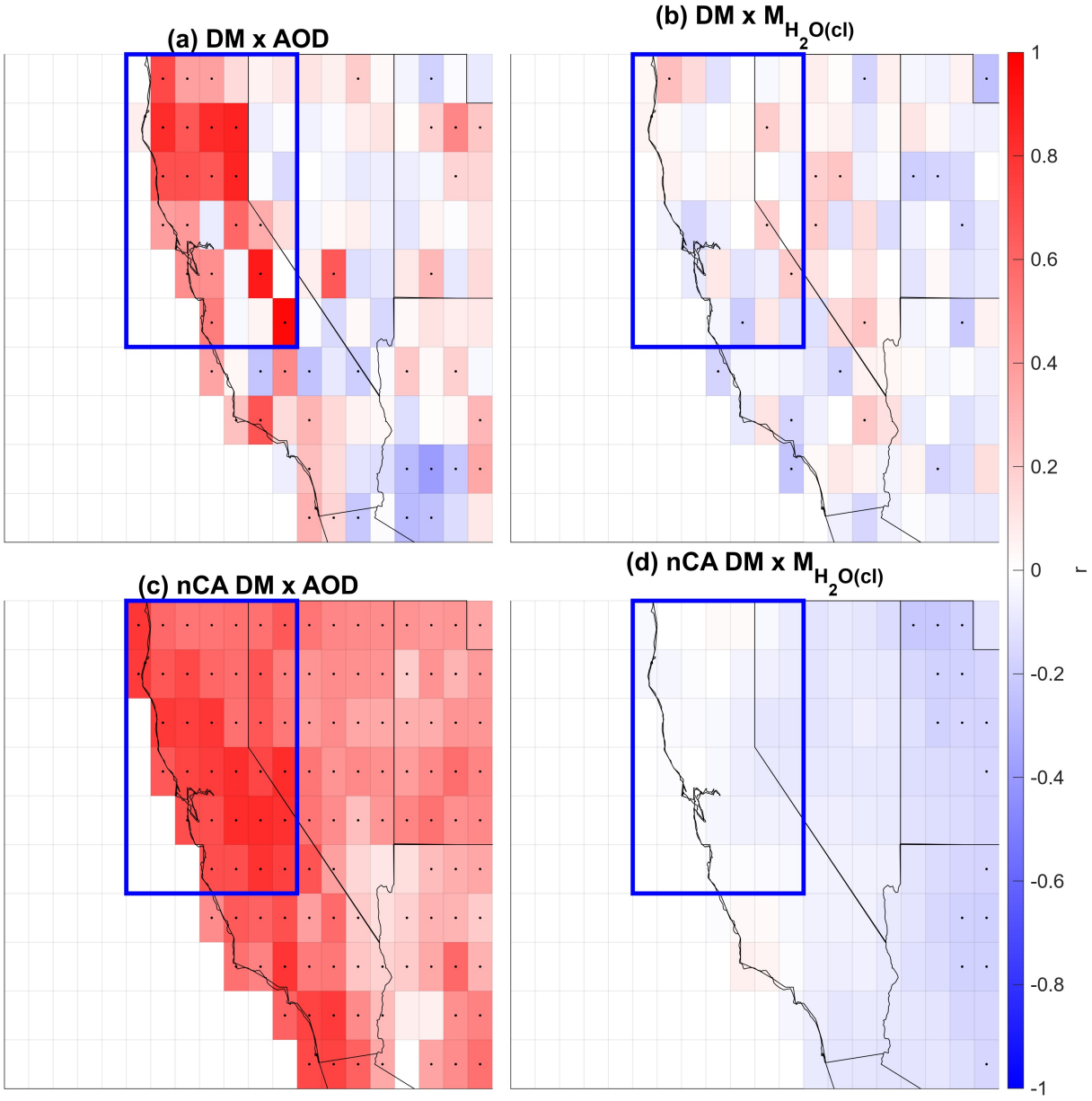

Figure S4. 2003-2022 June-October monthly cross correlations between fire dry matter emissions DM and variables that may indicate presence of fire using two different methods. The five months in each fire season were spliced together to generate a time series for each variable. (a,b) were generated using a gridcell-by-gridcell approach, where DM was correlated with (a) aerosol optical depth AOD and (b) 700-250hPa water mass mixing ratio $M_{H_2O(cl)}$ at each gridcell. (c,d) were generated using a similar method, but instead cross correlating northern California (nCA) regional average DM with (a) AOD and (b) $M_{H_2O(cl)}$. r represents the Pearson cross correlation coefficient. Black dots represent statistical significance at the 90% confidence interval using a two tailed test

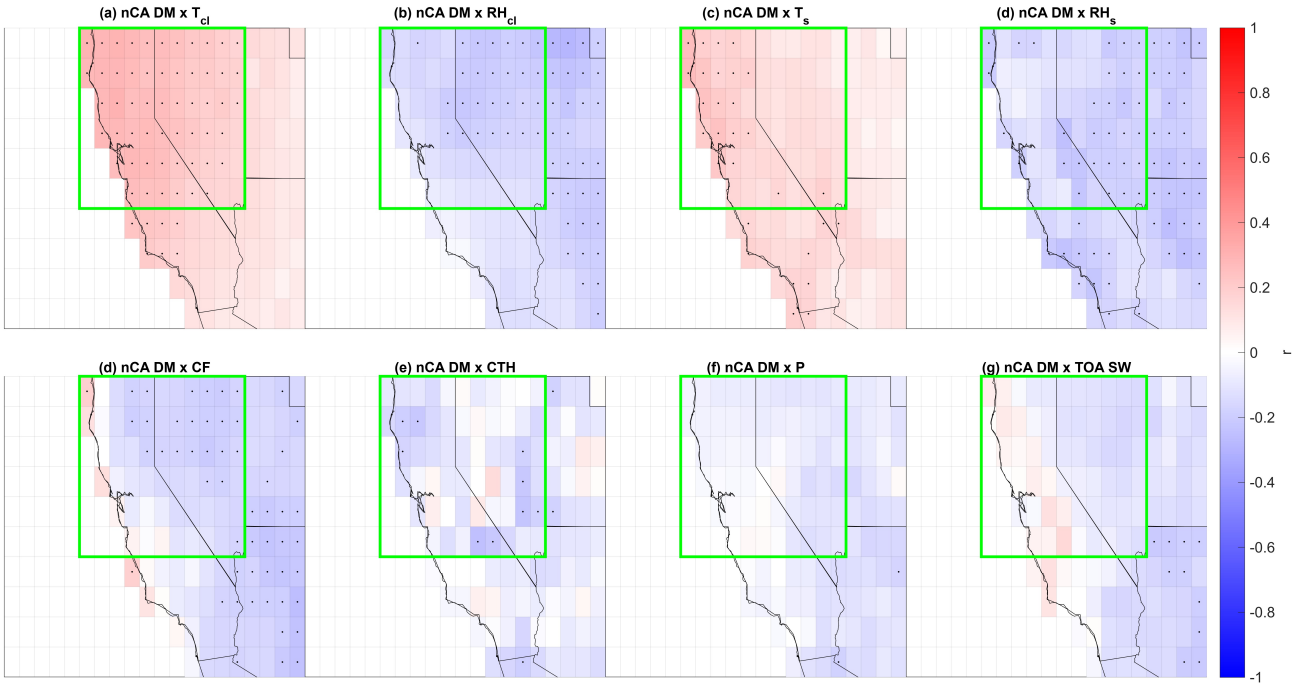

Figure S5. 2003-2022 June-October monthly cross correlations between northern California (nCA) regional average wildfire dry matter emissions DM and the meteorological variables. Includes (a) cloud layer (700-250hPa) temperature T, (b) cloud layer relative humidity RH, surface temperature T_s, surface relative humidity RH_s, cloud fraction CF, cloud top height CTH, precipitation P, and outgoing top of atmosphere shortwave radiation TOA. Black dots represent statistically significant cross correlation values at the 90% confidence interval using a two-tailed test. Sign and significance of cross correlations are generally consistent with **Figure 9**.

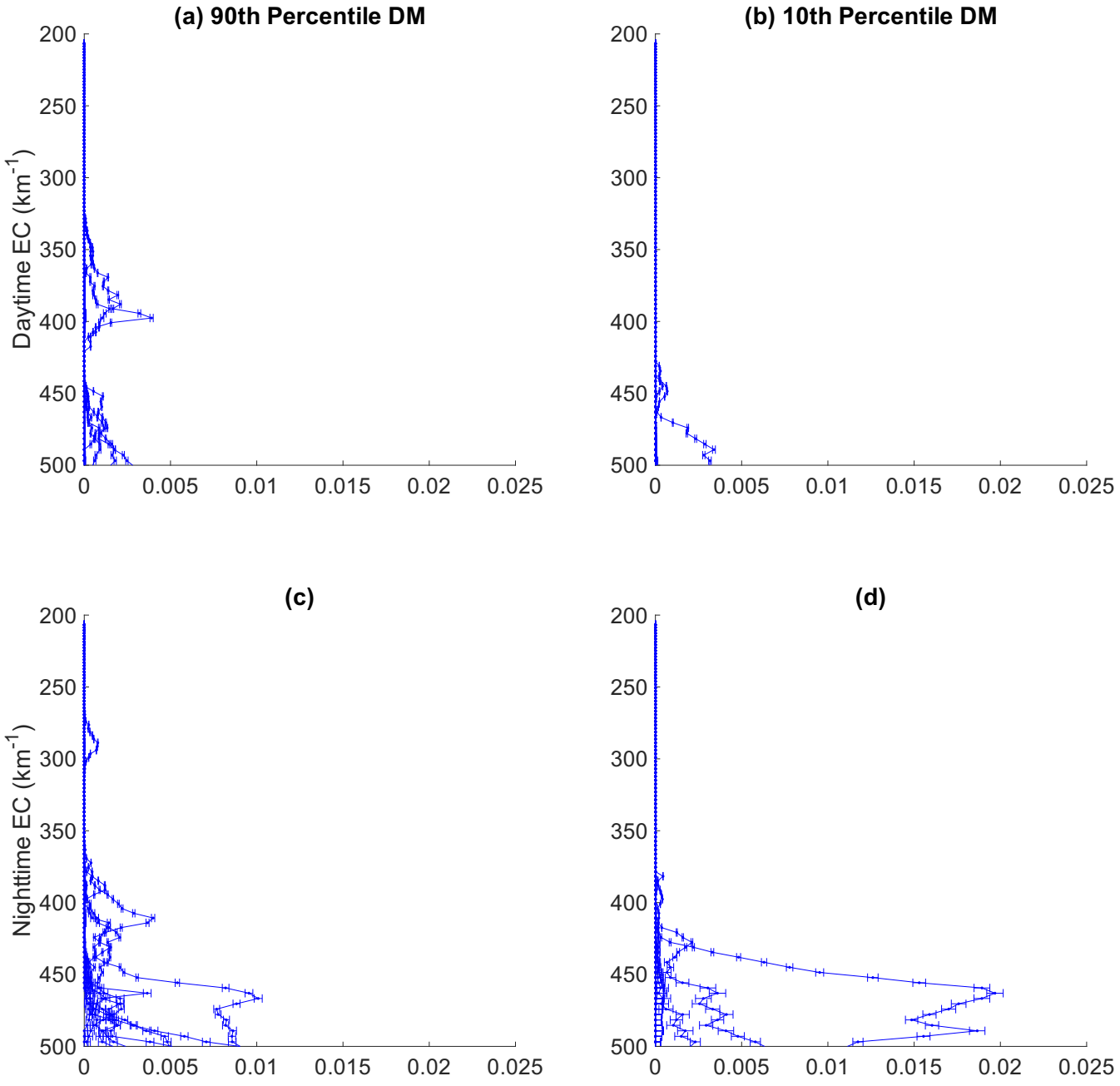

Figure S6. Stratified temporal-regional average CALIPSO vertical extinction coefficient (EC) profiles for smoke in the upper troposphere (500-200hPa) over the northern California-Nevada (nCA-NV) region in the 2003-2022 June-October time frame. Profiles both daytime (a,b) and nighttime (c,d) profiles for 90th percentile dry matter fire emission (DM) months (a,c) and 10th percentile DM months (b,d). Error bars represent standard error. Of note are that in both the daytime and nighttime profiles there is significant smoke aerosol in the 90th percentile daytime and nightime profiles above 400hPa, which is at a higher elevation than any EC in the 10th percentile profiles. Also of note is a significantly higher smoke EC retrieval at roughly 500hPa-425hPa in the nighttime retrieval, which may be from smoke transported from an area outside of nCA-NV during a 10th percentile month.

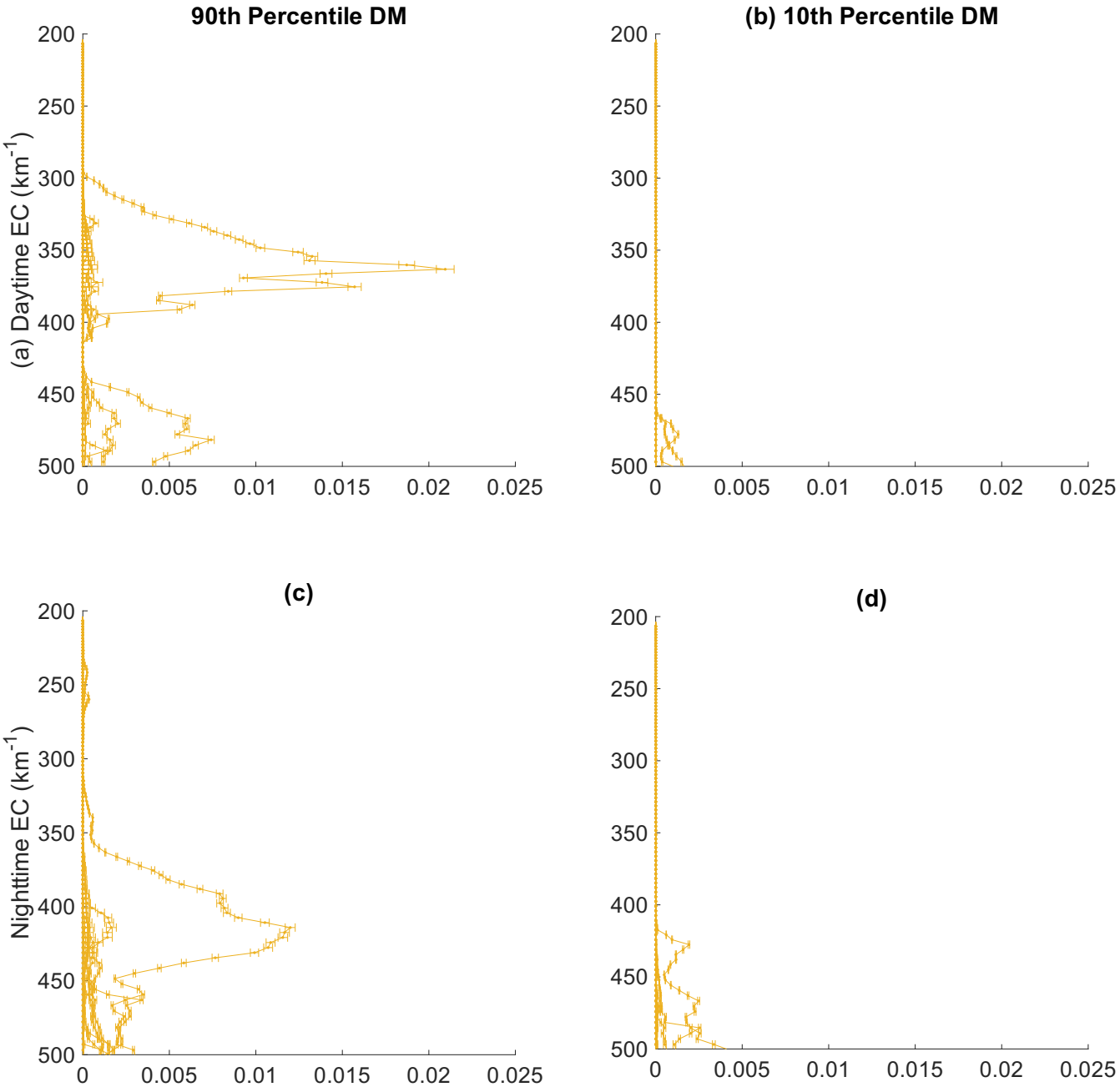

Figure S7. Stratified temporal-regional average CALIPSO vertical extinction coefficient (EC) profiles for polluted dust in the upper troposphere (500-200hPa) over the northern California-Nevada (nCA-NV) region in the 2003-2022 June-October time frame. Profiles both daytime (a,b) and nighttime (c,d) profiles for 90th percentile dry matter fire emission (DM) months (a,c) and 10th percentile DM months (b,d). Error bars represent standard error. Of note are that in both the daytime and nighttime profiles there is significantly larger polluted dust aerosol in the 90th percentile daytime and nightime profiles than anywhere in the 10th percentile profiles. Additionally, in 90th percentile DM months, significant polluted dust EC retrievals are found above 400hPa, where polluted dust EC is zero during 10th percentile DM months.

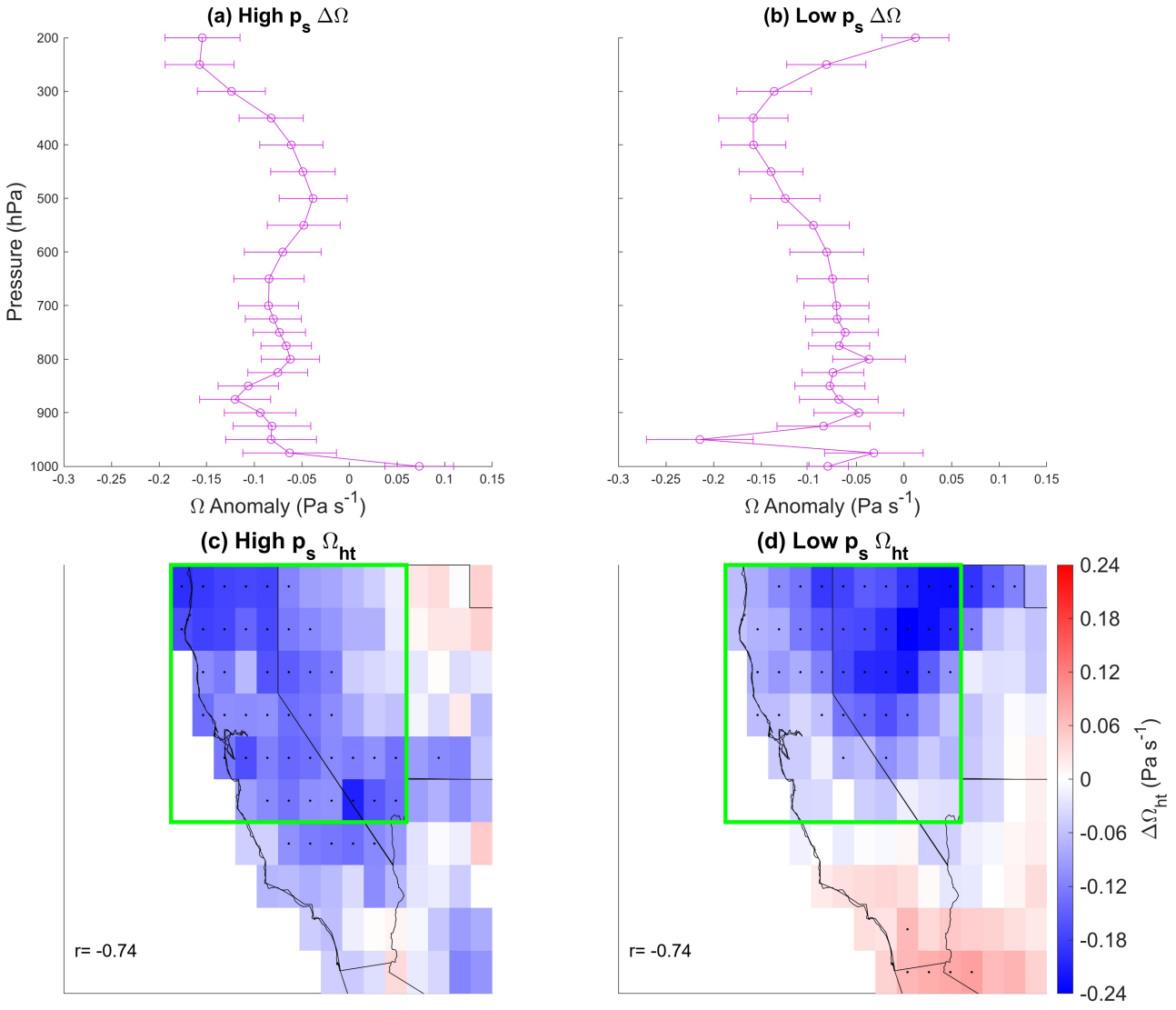

Figure S8. Responses in the vertical pressure velocity Ω profile to large fires compared to low fire extremes under high and low surface pressure p_s extremes and corresponding spatial responses. (a,b) Northern California-Nevada (nCA-NV) regional-temporal average differences in Ω between high (90th percentile) and low (10th percentile) northern California (nCA) fire dry matter emissions DM anomalies stratified by days of (a) high and (b) low p_s anomaly extremes in the 2003-2022 June-October time frame. (c,d) Difference between temporal average high troposphere (500-200hPa) vertical pressure velocity Ω_{ht} on high northern California (nCA) fire dry matter DM emission days and low nCA DM emission days that occur on (c) high and (d) low surface pressure p_s days in the 2003-2022 June-October time frame. Black dots represent statistically significant differences at the 90% confidence interval. Green box represents the northern California-Nevada region. Error bars represent standard error.

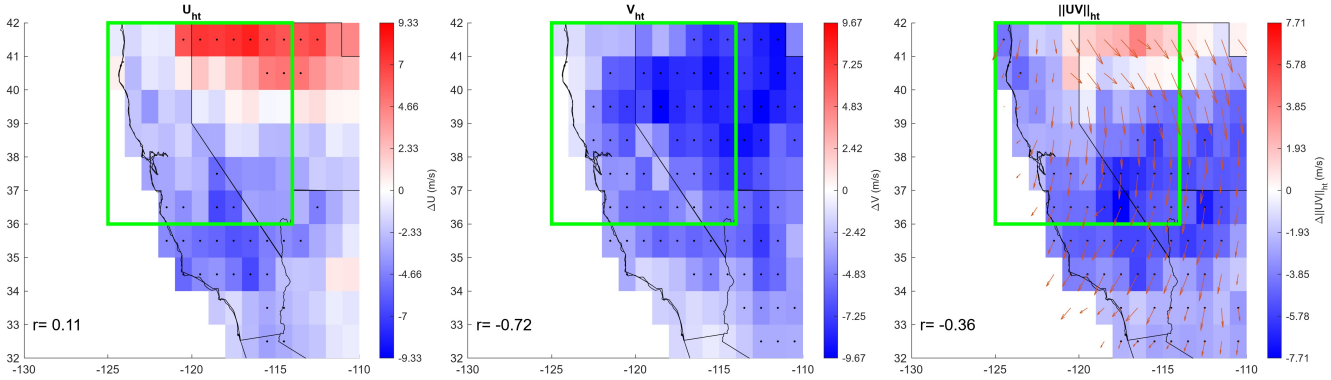

Figure S9. High troposphere (500-200hPa) wind anomalies during northern California (nCA) anomalously large fire days compared to anomalously fire days during low surface pressure p_s extremes in the 2003-2022 June-October time frame. Fire season high (90th percentile) minus low (10th percentile) nCA fire dry matter emissions days' high troposphere (a) longitudinal wind speed U_{ht} anomalies, (b) latitudinal wind speed V_{ht} anomalies, and (c) wind vector plot with length of vectors and the color of gridcell representing magnitude of wind speed anomalies. Arrows represent wind vector anomalies. Black dots represent statistically significant differences at the 90% confidence interval. Green box represents the northern California-Nevada region.

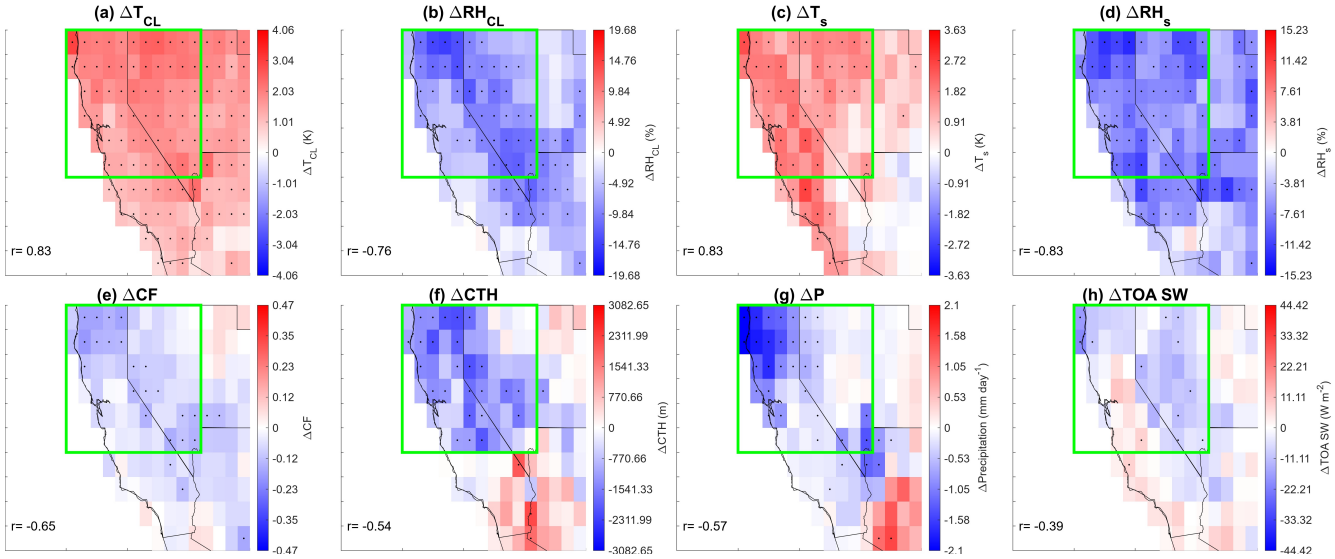

Figure S10. Meteorological responses under high versus low fire days with simultaneously high surface pressure. Difference between average variable anomalies on high (90th percentile) northern California (nCA) fire dry matter DM emission days and low (10th percentile) nCA DM emission days that occur on high surface pressure p_s days in the 2003-2022 June-October time frame. Variables include (a) 700hPa-250hPa average Temperature T_{cl}, 700hPa-250hPa average relative humidity RH_{cl}, (c) surface temperature T_s, (d) surface relative humidity RH_s, (e) cloud fraction CF, (f) cloud top height CTH, (g) precipitation, and (e) top of atmosphere TOA shortwave SW flux. Black dots represent statistically significant differences at the 90% confidence interval according to a two tailed test. Green box symbolizes the northern California-Nevada region. Pearson cross correlation r values in the top left corner of each plot represent the spatial correlation between MODIS Deep Blue aerosol optical depth AOD anomaly and the variable anomaly depicted in the figure. All values of r are significant at the 90% confidence interval according to a two-tailed test.

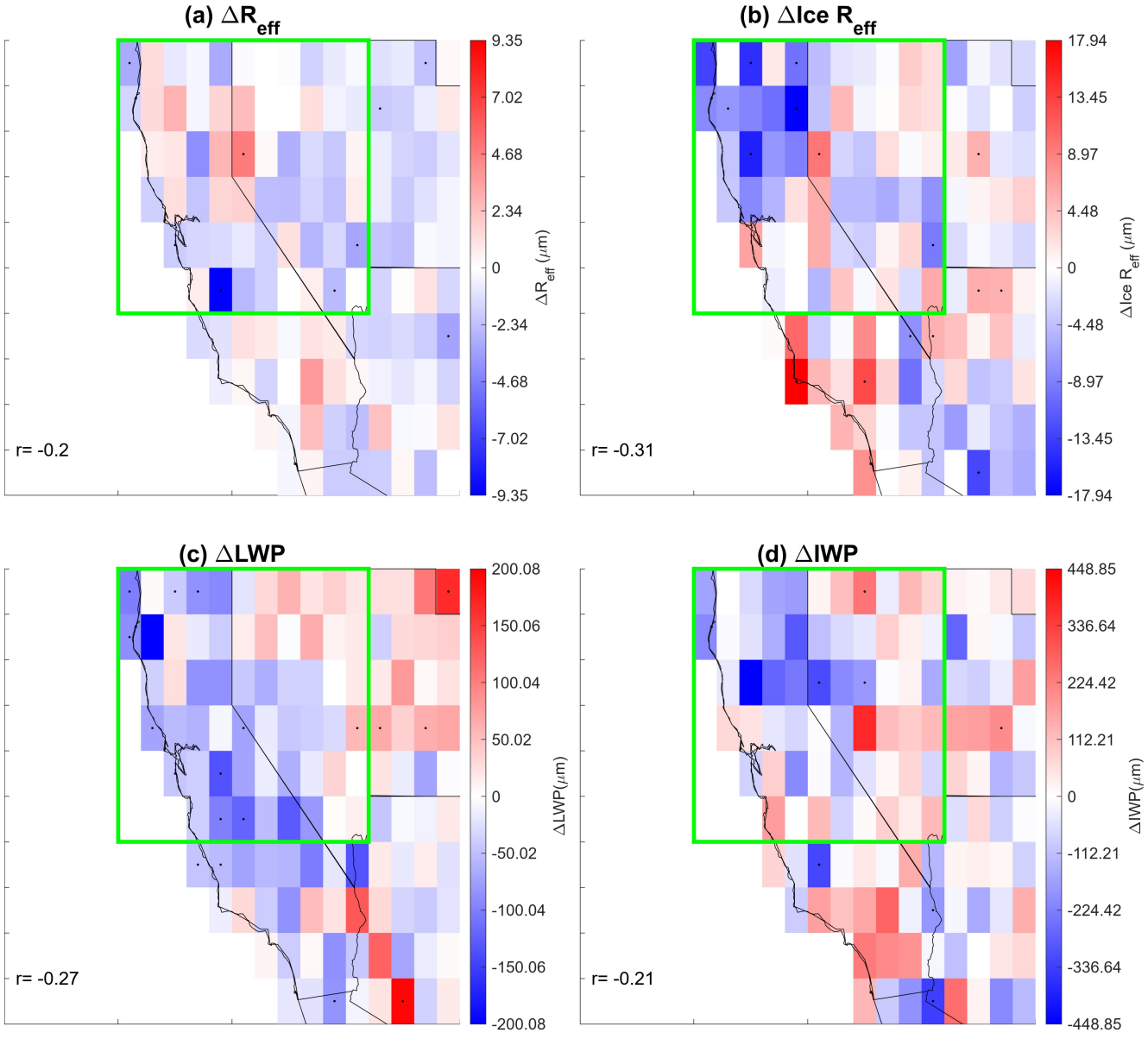

Figure S11. Cloud microphysical responses under high versus low fire days with simultaneously low surface pressure. Difference between temporal average variable anomalies on high (90th percentile) northern California (nCA) fire dry matter DM emission days and low (10th percentile) nCA DM emission days that occur on low surface pressure p_s days in the 2003-2022 June-October time frame. Variables include (a) liquid water effective radius R_{eff}, (b) ice R_{eff}, (c) liquid water path LWP, and (d) ice water path IWP. Black dots represent statistically significant differences. The green rectangle represents the northern California-Nevada region. r represents Pearson cross correlation coefficient values for cross correlations between aerosol optical depth and the variable of interest.

References

Gelaro, R., McCarty, W., Suárez, M. J., Todling, R., Molod, A., Takacs, L., Randles, C. A., Darmenov, A., Bosilovich, M. G., Reichle, R., Wargan, K., Coy, L., Cullather, R., Draper, C., Akella, S., Buchard, V., Conaty, A., Silva, A. M. d., Gu, W., Kim, G.-K., Koster, R., Lucchesi, R., Merkova, D., Nielsen, J. E., Partyka, G., Pawson, S., Putman, W., Rienecker, M., Schubert, S. D., Sienkiewicz, M., & Zhao, B. (2017). The Modern-Era Retrospective Analysis for Research and Applications, Version 2 (MERRA-2). *Journal of Climate*, 30(14), 5419–5454. Publisher: American Meteorological Society Section: Journal of Climate.

Global Modeling And Assimilation Office & Pawson, S. (2015). MERRA-2 inst3_3d_asm_np: 3d,3-Hourly,Instantaneous,Pressure-Level,Assimilation,Assimilated Meteorological Fields V5.12.4.

Kim, B. & Sarkar, S. (2017). Impact of wildfires on some greenhouse gases over continental USA: A study based on satellite data. *Remote Sensing of Environment*, 188, 118–126.

Liu, Y., Goodrick, S., & Heilman, W. (2014). Wildland fire emissions, carbon, and climate: Wildfire–climate interactions. *Forest Ecology and Management*, 317, 80–96.